Modelling Cloud Contamination in IASI Spectra

Maiurie Rasakulasuriar
St Hilda's College, University of Oxford
Supervised by Dr. A. Dudhia

Abstract

Retrieval algorithms for atmospheric composition typically require cloud-free conditions, leading to the rejection of partially cloudy footprints and a significant loss of data. In this report, we assess whether the measured radiance in a partially cloudy satellite footprint can be treated as a weighted average of clear-sky and cloudy radiation. Radiance measurements and cloud fractions from the Advanced Very High Resolution Radiometer (AVHRR) and the Infrared Atmospheric Sounding Interferometer (IASI) are used to evaluate the model. Clear-sky brightness temperatures from the two instruments show strong agreement, with a mean bias of approximately 0.23 K. When applying the model to partially cloudy scenes, the IASI cloud fraction provides the best agreement with observed cloud radiance. In contrast, the optimal cloud fraction derived from the model is more closely aligned with the AVHRR cloud fraction. Although the linear model captures the general effects of cloud contamination, it fails to account for variability in cloud optical thickness and the nonlinear radiative effects associated with unresolved cloud inhomogeneity.

I. INTRODUCTION

Satellite infrared remote sensing plays a central role in meteorology and climate research [1], providing global observations of atmospheric temperature and composition. Infrared sounders have been used since the 1970s to retrieve vertical temperature profiles and gas concentrations. However, clouds significantly alter the infrared radiation measured by satellites at the top of the atmosphere by obscuring surface emission and by introducing colder cloud-top emission [2].

The Infrared Atmospheric Sounding Interferometer (IASI), onboard the MetOp-A, B, and C satellites, measures infrared radiances across a wavenumber range of 645 to 2760 cm^{-1} and resolves absorption features of trace gases such as ozone, methane, ammonia, and carbon monoxide, enabling their retrieval from the observed spectra. The primary application of IASI is the retrieval of atmospheric temperature and water vapour profiles, which are required with high accuracy for numerical weather prediction models.

However, the relatively coarse spatial resolution of IASI (∼12 km at nadir, i.e. directly beneath the satellite) means that many footprints are partially cloud-covered. Most current retrieval algorithms assume horizontal homogeneity within each footprint and therefore require a cloud fraction of 0%, leading to partially cloudy footprints being discarded.

For numerical weather prediction, where high accuracy is required and alternative observations are available, a cloud fraction threshold of 0% is acceptable. In contrast, for retrievals of short-lived trace gases, spatial coverage is often more important than absolute accuracy, as these species exhibit strong local variability. Therefore, discarding partially cloudy footprints can lead to substantial data loss.

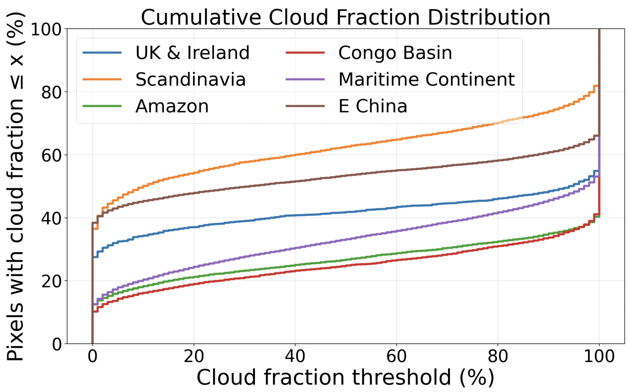

Figure 1: Cumulative distribution of cloud fraction for selected regions (defined in Appendix A). Each curve shows the percentage of footprints with a cloud fraction $\leq x$, where x is the cloud-fraction threshold. Persistently cloudy regions (e.g. the Congo Basin) exhibit a much lower proportion of cloud-free footprints, highlighting the loss of usable data.

This effect is particularly severe in persistently cloudy regions: Fig. 1 shows that only around 36% of IASI footprints in Scandinavia and as few as 10% of the footprints in the Congo Basin are cloud-free. This loss of data significantly reduces spatial coverage and may introduce biases into atmospheric retrievals.

A potential solution is provided by complementary high-resolution imagers such as the Advanced Very High Resolution Radiometer (AVHRR). While AVHRR has lower spectral resolution than IASI, its finer spatial resolution ($\sim$1 km) enables the estimation of cloud fraction and cloud-top temperature within an IASI footprint. These additional constraints provide an opportunity to separate and model the clear-sky and cloudy radiance contributions within partially cloudy footprints. If successful, this approach could significantly increase the amount of data usable in retrieval algorithms.

Previous studies [3, 4] model the radiance in a partially cloudy footprint as a weighted linear combination of clear-sky and fully cloudy radiances. In this study, we assess whether a linear radiance mixing model can accurately represent partially cloudy IASI footprints by applying it to cases with cloud fractions between 25% and 75%, and evaluating its sensitivity to both IASI and AVHRR cloud fractions.

The remainder of this paper is structured as follows. Section II introduces the Planck function. Section III describes the IASI and AVHRR instruments. Section IV compares the measured radiances of AVHRR and IASI in cloud-free scenes, to validate our study's approach of combining radiance measurements from both instruments. Section V explains the linear model used in partially cloudy footprints, and the data selection is explained in Section VI. Section VII analyses the results of our linear model for two different estimations of cloud fraction in the IASI footprint. Section VIII compares which cloud fraction estimation is best suited for our linear model. Finally, Section IX summarises our findings.

II. PLANCK'S FUNCTION

Satellite instruments, such as IASI and AVHRR, measure spectral radiance. In the thermal infrared, this radiation is primarily due to thermal emission from the Earth's surface, clouds, and atmospheric gases.

Thermal emission from an idealised blackbody is described by Planck's law. In wavenumber form, the spectral radiance of a blackbody at temperature T is given by

$$B_{\tilde{\nu}}(T) = \frac{2hc^2\tilde{\nu}^3}{\exp\left(\frac{hc\tilde{\nu}}{kT}\right) - 1}, \tag{1}$$

where h is Planck's constant, c is the speed of light, k is Boltzmann's constant, and $\tilde{\nu}$ is the wavenumber.

For temperatures typical of the Earth's surface (200–300 K), Wien's displacement law indicates that the peak of thermal emission lies in the infrared, which explains why this spectral region is well suited to atmospheric sounding. Without an atmosphere, the spectrum would follow a Planck curve corresponding to the surface temperature. However, atmospheric absorption and emission modify this spectrum before it reaches the satellite.

In the absence of clouds, the observed infrared spectrum (Fig. 2) is shaped by molecular absorption and emission within the atmosphere. Gases such as H_2O, CO_2, and O_3 absorb radiation at specific wavelengths, producing characteristic features superimposed on a Planck-like continuum. These features reduce the observed radiance relative to the surface emission, leading to lower brightness temperatures at specific wavenumbers.

III. INSTRUMENTS

1. IASI

The Infrared Atmospheric Sounding Interferometer (IASI) is a Fourier transform spectrometer that measures infrared radiation emitted from the Earth's surface, atmosphere, and cloud tops. Its high spectral resolution enables individual molecular absorption features to be resolved, which is essential for retrieving atmospheric temperature and composition.

IASI operates over a spectral range of 645–2940 cm^{-1} (equivalently 3.4–15.5 µm). In this work, analysis is restricted to the atmospheric window region 700–1000 cm^{-1} (approximately 10–14.3 µm) to avoid strong absorption bands, such as CO_2 at around 620–720 cm^{-1} and a major H_2O vibrational band around 1300–2000 cm^{-1}. In the 700–1000 cm^{-1} region, absorption by water vapour and other gases is relatively weak, allowing radiation from the surface and lower atmosphere to dominate.

IASI measures spectral radiance $L_{\tilde{\nu}}$ at the top of the atmosphere for each footprint. Atmospheric properties such as temperature and gas concentrations are not measured directly, but are instead retrieved from these observed radiances using radiative transfer modelling.

The instrument has a spatial footprint of around 12 km in diameter at nadir, meaning that individual footprints often contain a mixture of clear and cloudy regions, making the interpretation of ob-

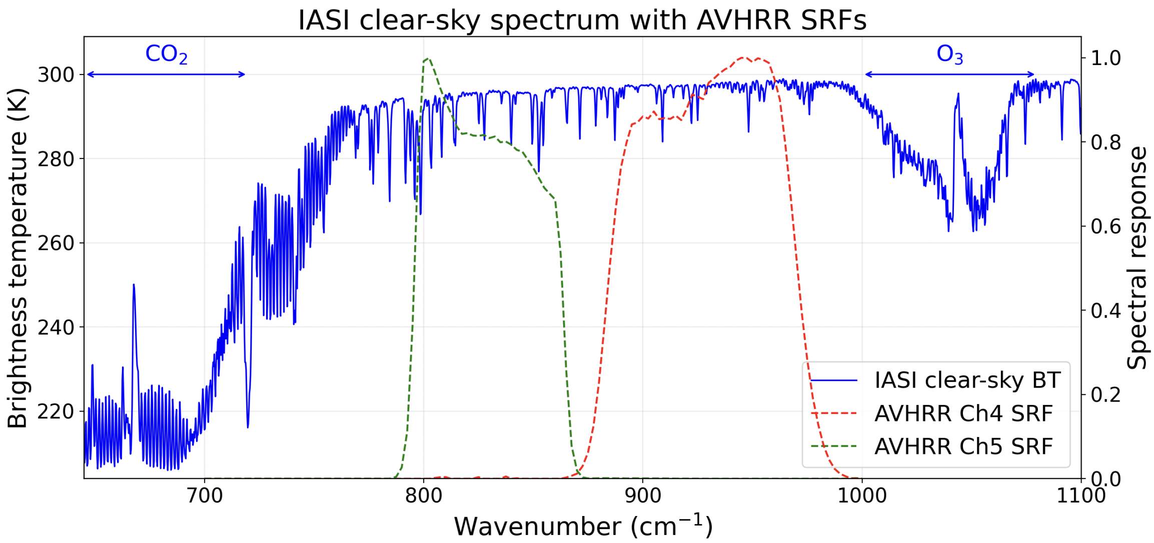

Figure 2: IASI clear-sky brightness temperature spectrum (blue line) in the 700–1000 cm^{-1} window, with AVHRR spectral response functions (SRFs) for Channels 4 (red dashed line) and 5 (green dashed line) overlaid. The spectrum follows a Planck-like envelope corresponding to surface emission, but exhibits absorption features due to atmospheric gases. Strong bands [5] from CO_2 (∼645–720 cm^{-1}) and O_3 (∼1000–1080 cm^{-1}) reduce the observed brightness temperature, while numerous smaller-scale features between these bands arise primarily from weaker H_2O absorption lines. The AVHRR spectral response functions [6] were interpolated to match the IASI spectral resolution (0.25 cm^{-1}) and renormalised.

served radiances more complex. This spatial inhomogeneity within the footprint is a key challenge addressed in this study.

In addition to spectral radiances $L_{\tilde{\nu}}$, the IASI data include the fraction of cloud coverage within a spatial footprint (f_{IASI}).

2. AVHRR

The Advanced Very High Resolution Radiometer (AVHRR) is an imaging instrument flown on the same MetOp satellites as IASI. Each IASI footprint (∼ 12 km) contains many higher-resolution AVHRR pixels (∼ 1 km), each with an associated radiance measurement. Hereafter, "footprint" refers to the IASI scene (∼ 12 km), while "pixel" refers to the higher-resolution AVHRR measurements (∼ 1 km). Within a given footprint, these AVHRR radiances are grouped into clusters of similar radiance values by the AVHRR processing algorithm. For each cluster, the mean radiance (`rav`) is computed, along with its fractional coverage (`pct`), defined as the proportion of AVHRR pixels within the IASI footprint belonging to that cluster.

The total number of radiance clusters within an IASI footprint is provided as the flag `ncl`. Appendix B defines all of the IASI and AVHRR flags used in this study.

AVHRR measures radiance in a small number of broad spectral channels spanning the visible and infrared. Since this study focuses on the atmospheric window region (∼10–14.3 µm), we are interested in AVHRR Channel 4 (10.3–11.3 µm), and Channel 5 (11.5–12.5 µm).

The AVHRR Spectral Response Function (SRF) describes how sensitive each sensor channel is to radiation across different wavelengths (Fig. 2). Rather than measuring radiance at a single wavelength, each AVHRR channel detects radiation over a finite spectral range, with varying sensitivity across that range. The SRF quantifies this sensitivity, is normalised between 0 and 1, and effectively acts as a weighting function applied to the incoming radiance.

IV. COMPARISON OF IASI AND AVHRR IN HOMOGENEOUS CLOUD-FREE SCENES

To validate the consistency between instruments, we assume that cloud-free ocean footprints are homogeneous and therefore contain a single radiance cluster (ncl=1), i.e. all AVHRR pixels within the footprint have similar (though not identical) radiances. The IASI radiance in this footprint can then be compared to the mean AVHRR radiance of that cluster.

Since AVHRR measures band-integrated radiances in different channels, the high-resolution IASI spectra are integrated over the spectral response function (SRF). In this study, we refer to the resulting SRF-weighted radiance as the convolved IASI radiance. This is given by

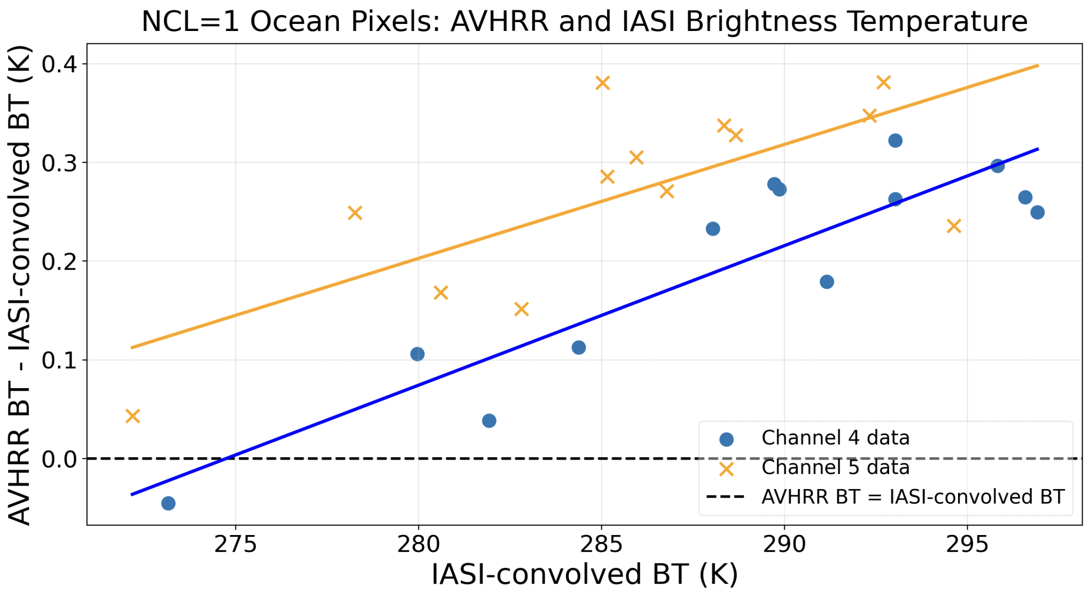

Figure 3: Brightness temperature (BT) residuals (AVHRR − IASI) as a function of IASI-convolved brightness temperature for cloud-free ocean footprints identified as homogeneous single-cluster scenes ($\texttt{ncl} = 1$). For each footprint, the mean AVHRR brightness temperature of the cluster is compared with IASI radiances convolved with the AVHRR spectral response functions and converted to brightness temperature. Linear fits are shown for both channels: Channel 4: $\Delta T = (0.014 \pm 0.002)\, T_{\mathrm{IASI}} - (3.9 \pm 0.6)$, Channel 5: $\Delta T = (0.012 \pm 0.003)\, T_{\mathrm{IASI}} - (3.0 \pm 0.9)$.

$$R = \frac{\int L_{\tilde{\nu}}(\tilde{\nu})\, \mathrm{SRF}(\tilde{\nu})\, d\tilde{\nu}}{\int \mathrm{SRF}(\tilde{\nu})\, d\tilde{\nu}}, \tag{2}$$

where R is the convolved IASI radiance, and $L_{\tilde{\nu}}(\tilde{\nu})$ is the measured IASI spectral radiance. We therefore expect R to be consistent with the mean AVHRR radiance of the single cluster in a cloud-free IASI footprint.

Since the Planck function (Eqn. 1) is non-linear in temperature, all analysis is performed in radiance space, with final results converted to brightness temperature for ease of interpretation.

Fig. 3 shows the brightness temperature residuals (AVHRR − IASI) as a function of IASI-convolved brightness temperature for both channels. The mean residuals are 0.198 K for Channel 4 and 0.268 K for Channel 5, with root mean square errors (RMSE) of 0.225 K and 0.284 K, respectively. The small mean residuals and low RMSE values indicate good agreement between the two instruments in homogeneous, cloud-free scenes.

The fitted residual gradients are small (0.014 ± 0.002 for Channel 4 and 0.012 ± 0.003 for Channel 5), indicating a weak temperature dependence. The negative intercepts (-3.9 ± 0.6 K and -3.0 ± 0.9 K) indicate a slight systematic offset between the instruments, with AVHRR brightness temperatures tending to be slightly lower than the convolved IASI values. This offset may arise from the interpolation of the spectral response functions from a 0.1 cm^{-1} grid to 0.25 cm^{-1}.

Overall, the differences in brightness temperature between IASI and AVHRR are small, indicating that the spectral convolution of IASI radiances into AVHRR-equivalent channels (Eqn. 2) is performing as expected.

V. MODELLING PARTIALLY CLOUDY FOOTPRINTS

If a fraction f of an IASI footprint is covered by cloud and the remainder is cloud-free, the measured spectral radiance may be approximated as the area-weighted sum of cloudy and clear-sky contributions:

$$L_{\tilde{\nu}}^{\mathrm{mix}} = f L_{\tilde{\nu}}^{\mathrm{cloud}} + (1 - f) L_{\tilde{\nu}}^{\mathrm{clear}}, \tag{3}$$

where $L_{\tilde{\nu}}^{\mathrm{mix}}$ is the observed spectral radiance in a partially cloudy footprint, and $L_{\tilde{\nu}}^{\mathrm{cloud}}$ and $L_{\tilde{\nu}}^{\mathrm{clear}}$ are the cloudy and clear-sky components, respectively.

Fig. 4 illustrates a simplified representation of a partially cloudy footprint, in which a fraction f of the footprint is covered by cloud and the remaining fraction $(1 - f)$ is cloud-free. The cloudy fraction and the clear-sky fraction can be treated as two independent radiative components ($\texttt{ncl} = 2$).

In the infrared window region, optically thick clouds behave approximately as blackbody emitters, since their emissivity approaches one ($\varepsilon_{\tilde{\nu}} \approx 1$). The radiance from a fully cloud-covered footprint may therefore be approximated as

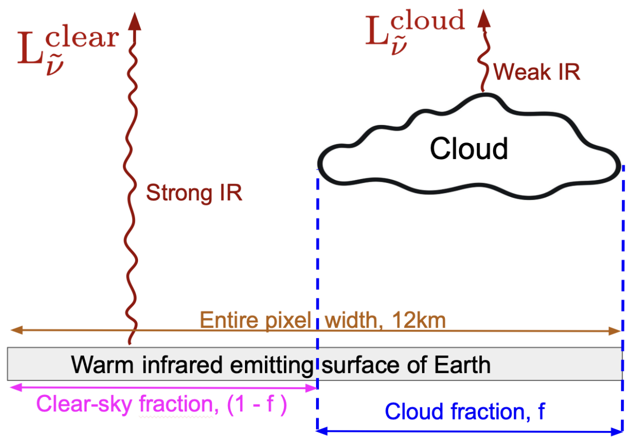

Figure 4: Schematic representation of a partially cloudy IASI footprint, and our definition of cloud fraction, f.

$$L_{\tilde{\nu}}^{\text{cloud}} \approx B_{\tilde{\nu}}(T_{\text{cloud}}), \tag{4}$$

where $B_{\tilde{\nu}}$ is the spectral radiance emitted by an ideal blackbody at the cloud-top temperature T_{cloud}.

The simple linear radiance mixing model assumes a single-layered uniform cloud within the footprint (Fig. 4). Therefore, only footprints classified as `ncl` $= 2$ were considered in this study. Footprints with more complex cloud structures (`ncl` ≥ 3) were excluded, as multiple layers of clouds would introduce additional unknown radiative components.

1. Defining cloud fraction f

Section III.1 defines f_{IASI} as the fraction of cloud coverage within an IASI footprint.

Alternatively, a cloud fraction can be estimated from the AVHRR clustering algorithm. In a partially cloudy footprint (`ncl` $= 2$), the cluster with the lower mean radiance is typically interpreted as the cloudy component, while the warmer cluster represents the clear-sky portion of the scene. The cloud fraction f_{AVHRR} is therefore defined as the fraction of AVHRR pixels assigned to the colder cluster within the IASI footprint.

The AVHRR clustering algorithm groups pixels according to radiance rather than physical cloud properties. As a result, pixels containing semi-transparent clouds, although physically cloudy, can exhibit relatively warm radiances and be misclassified into the clear-sky cluster rather than the cloud cluster. Therefore, f_{AVHRR} does not represent a true physical cloud fraction, but rather a radiance-based partitioning of the scene.

In contrast, f_{IASI} is based on explicit cloud detection and is therefore expected to be more physically representative of the true cloud fraction.

The choice of cloud fraction definition strongly influences the accuracy of the radiance mixing model.

VI. DATA SELECTION

IASI observes the Earth by scanning across the satellite's ground track as it moves along its orbit. During each scan line, the instrument records measurements at 30 positions across the satellite track. At each position, four individual IASI footprints are measured in a 2×2 configuration (Fig. 5), resulting in 120 footprints per scan line.

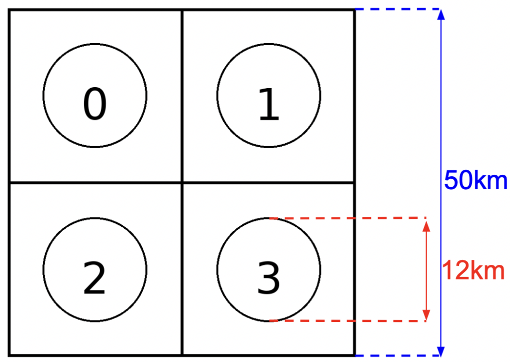

Figure 5: Schematic representation of the IASI footprint structure showing the 2×2 instantaneous fields of view within a single scan position. Each circular footprint has a diameter of approximately 12 km.

In this study, observations were restricted to latitudes within $\pm30°$ to avoid complications associated with low surface temperatures and frequent atmospheric temperature inversions.

The analysis was restricted to oceanic scenes, where surface emissivity is more uniform than that over land. It is therefore assumed that differences in radiance between adjacent footprints arise primarily from cloud effects.

Towards the edges of the scan, IASI footprints become increasingly elliptical due to the slant viewing geometry. As a result, these edge footprints sample a larger area and are more likely to include spatial variability in surface and atmospheric conditions.

Furthermore, the cloud fraction f_{IASI}, in our partially cloudy footprints, was restricted to $0.25 \leq f_{\text{IASI}} \leq 0.75$ to clearly distinguish between cloud-free and fully cloudy footprints, and to avoid extreme cases where very small values of f amplify noise.

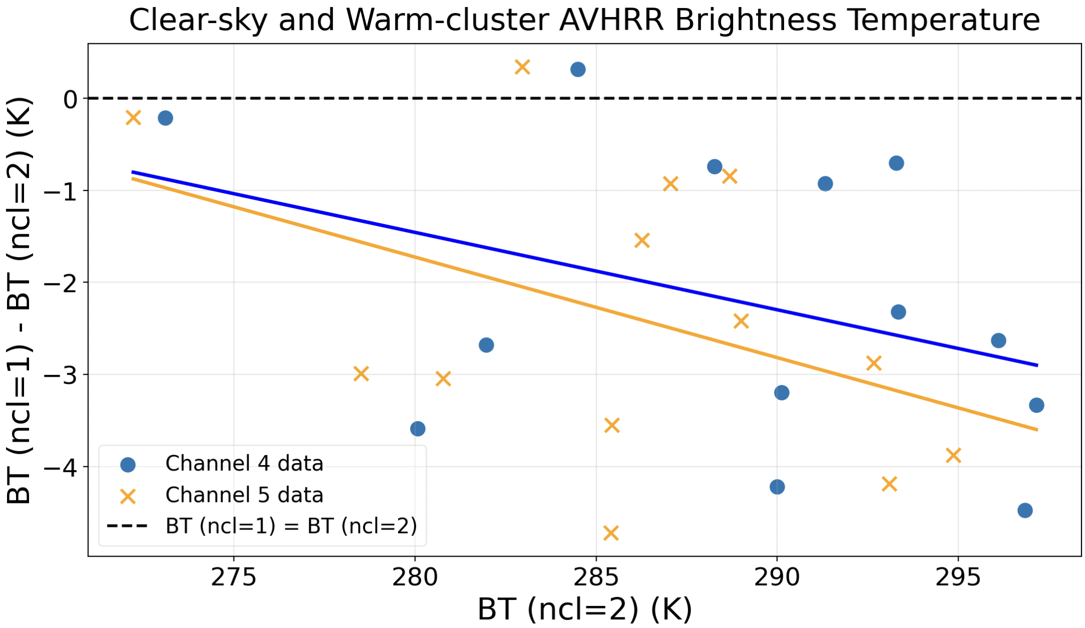

Figure 6: AVHRR brightness temperature (BT) residuals between clear-sky footprints ($\texttt{ncl} = 1$) and the warmer cluster in partially cloudy footprints ($\texttt{ncl} = 2$), plotted as a function of the AVHRR mean BT of the warm cluster. The AVHRR mean BT of the single cluster in a cloud-free footprint is compared with that of the warmer cluster in a neighbouring partially cloudy footprint. Linear fits are shown for both channels: Channel 4: $\Delta T = (-0.084 \pm 0.061)\, T_{\text{warm}} + (22.1 \pm 17.7)$, Channel 5: $\Delta T = (-0.109 \pm 0.069)\, T_{\text{warm}} + (28.9 \pm 19.9)$.

1. *Selecting Footprint Pairs*

To represent the components in our linear radiance model (Eqn. 3), we identified spatially adjacent footprint pairs in the same 2×2 instantaneous fields of view:

- A cloud-free footprint ($\texttt{ncl} = 1$, $f_{\text{IASI}} = 0$),
- A partially cloudy footprint ($\texttt{ncl} = 2$, $0.25 \leq f_{\text{IASI}} \leq 0.75$),

where the radiance in the cloud-free footprint is $L_{\tilde{\nu}}^{\text{clear}}$, the radiance in the partially cloudy footprint is $L_{\tilde{\nu}}^{\text{mix}}$, and f is the cloud fraction (Eqn. 3).

Since the selected footprints are spatially adjacent and lie over the ocean, atmospheric temperature profiles and gas concentrations are assumed to vary weakly between them. This assumption may break down in the presence of strong meteorological gradients, such as near atmospheric fronts or regions of rapidly varying temperature and humidity, where differences may not arise solely from cloud effects. However, restricting the analysis to low latitudes and oceanic regions reduces the likelihood of such gradients, so the assumption is expected to hold for the majority of selected footprint pairs.

By selecting adjacent footprint pairs, the radiance in the cloud-free footprint ($\texttt{ncl} = 1$, $f_{\text{IASI}} = 0$) is taken as a good approximation to the clear-sky component within the partially cloudy footprint ($\texttt{ncl} = 2$). The cluster with the higher mean radiance is therefore interpreted as the clear-sky radiative component, $L_{\tilde{\nu}}^{\text{clear}}$.

2. *Assumption for clear-sky homogeneity*

To test the assumption that the clear-sky component of a partially cloudy footprint is equivalent to a neighbouring clear-sky footprint, the AVHRR mean radiance of cloud-free footprints ($\texttt{ncl} = 1$) was compared with the warmer cluster in adjacent partially cloudy footprints ($\texttt{ncl} = 2$).

Fig. 6 shows the residuals between the AVHRR mean brightness temperatures of these two cases. The mean bias and root mean square error (RMSE) are -2.21 ± 2.68 K for Channel 4 and -2.37 ± 2.83 K for Channel 5, where the $\pm$ values denote the RMSE. The negative bias indicates that the warm cluster in partially cloudy footprints has a higher brightness temperature than adjacent clear-sky footprints.

This behaviour likely arises because the AVHRR clustering algorithm groups footprints based on radiance rather than physical cloud properties (Section V.1), allowing cloud-contaminated footprints to be included in the warm cluster. The relatively large scatter (up to 5 K) and negative gradients (-0.084 ± 0.061 for Channel 4 and -0.109 ± 0.069 for Channel 5) indicate a temperature-dependent bias, with residuals increasing in magnitude at higher

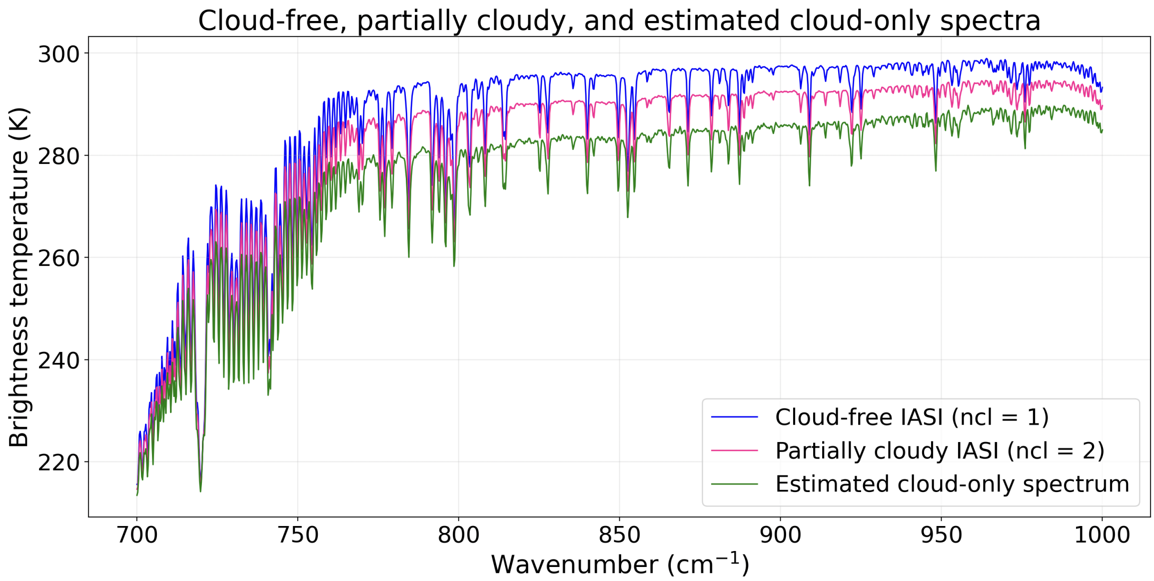

Figure 7: Brightness temperature spectra in the 700–1000 cm^{-1} window for a cloud-free footprint (`ncl` $= 1$, $f_{\text{IASI}} = 0$, blue), a partially cloudy footprint (`ncl` $= 2$, $f_{\text{IASI}} = 0.44$, pink), and the corresponding estimated cloud-only spectrum (green). The partially cloudy spectrum exhibits a lower continuum brightness temperature due to the contribution of colder cloud-top emission. The cloud-only spectrum is obtained by inverting the linear radiance mixing model (Eqn. 5) using the IASI cloud fraction.

brightness temperatures.

These results show that the assumption of equivalence between the clear-sky footprint and the clear component within partially cloudy footprints is only approximate.

VII. RECONSTRUCTION OF CLOUDY RADIANCES

Having validated the instrument consistency and clear-sky assumption, we now apply the linear radiance model (Eqn. 3) to reconstruct the cloud-component radiance, $L_{\tilde{\nu}}^{\text{cloud}}$, in partially cloudy footprints.

1. *Comparing $L_{\tilde{\nu}}^{clear}$ and $L_{\tilde{\nu}}^{mix}$*

Representative IASI brightness temperature spectra for a cloud-free footprint (`ncl` $= 1$) and a partially cloudy footprint (`ncl` $= 2$) are shown in Fig. 7 for the 700–1000 cm^{-1} window region.

In partially cloudy cases, the brightness temperature spectrum is lower than the cloud-free IASI spectrum due to colder cloud-top emission, while the overall spectral structure is largely preserved. This behaviour is consistent with linear mixing of clear-sky and cloudy radiances. The resulting suppression of the infrared continuum reduces the observed radiance and distorts the spectral signal used in trace-gas retrievals, highlighting the need to account for cloud contamination.

2. *Finding $L_{\tilde{\nu}}^{cloud}$*

Since the cloud fraction f is known from Section V.1, we can rearrange the linear radiance mixing relation (Eqn. 3) to obtain the cloudy component in our partially cloudy footprint:

$$L_{\tilde{\nu}}^{\text{cloud}} = \frac{L_{\tilde{\nu}}^{\text{mix}} - (1-f)L_{\tilde{\nu}}^{\text{clear}}}{f}. \quad (5)$$

For the example shown in Fig. 7, the radiance mixing equation (Eqn. 3) is inverted using the IASI cloud fraction ($f_{\text{IASI}} = 44.0\%$) to estimate the cloudy radiance $L_{\tilde{\nu}}^{\text{cloud}}$. The reconstructed spectrum exhibits lower brightness temperatures and enhanced absorption features, consistent with emission originating from higher, colder layers of the atmosphere.

The pronounced drop in brightness temperature around 700–750 cm^{-1} corresponds to the strong CO_2 absorption band. In this region, the observed radiation primarily originates from higher altitudes, often above the cloud top, so the cloud-free (blue) and partially cloudy (pink) spectra show little difference. However, the linear mixing model is applied uniformly across all wavelengths, leading to an estimated cloud-only spectrum that is systematically lower, even in spectral regions where the radiance is weakly influenced by the cloud layer. This demonstrates that the linear mixing model is less reliable within strong absorption bands.

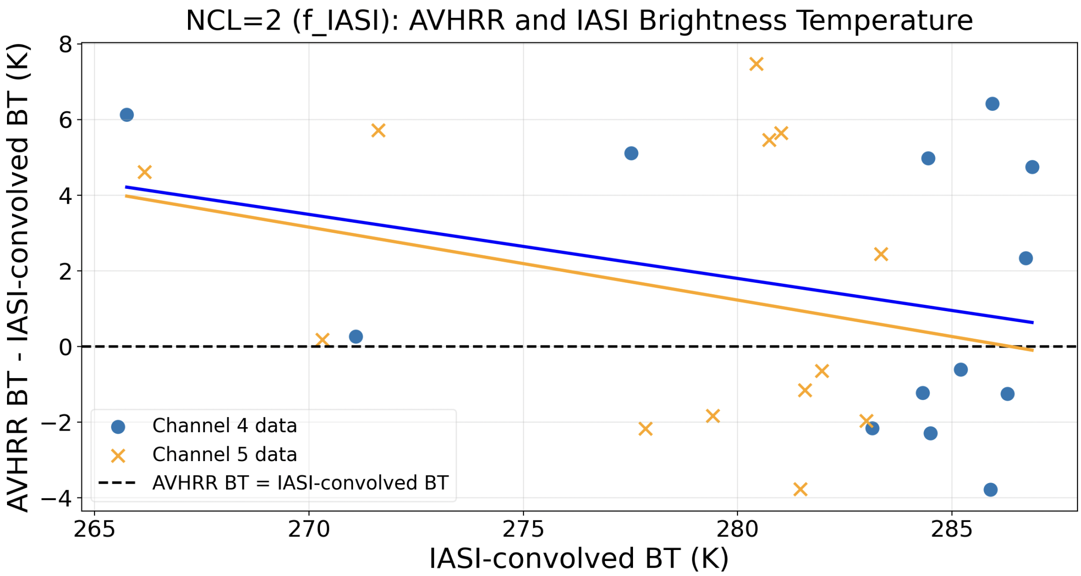

Figure 8: Brightness temperature (BT) residuals (AVHRR − IASI) for the cloud component in partially cloudy footprints (`ncl` = 2), plotted as a function of the IASI-convolved BT of the estimated cloud component. The AVHRR mean BT of the colder cluster is compared with the IASI BT obtained by inverting the linear radiance mixing model (Eqn. 5) using f_{IASI} as the cloud fraction. Linear fits are shown for both channels: Channel 4: $\Delta T = (-0.169 \pm 0.157)\, T_{\mathrm{IASI}} + (49.2 \pm 44.4)$, Channel 5: $\Delta T = (-0.193 \pm 0.203)\, T_{\mathrm{IASI}} + (55.2 \pm 56.5)$.

3. *Using $f = f_{\mathrm{IASI}}$*

In the previous section, the reconstructed cloudy radiance was obtained using f_{IASI} as the cloud fraction in Eqn. 5.

Fig. 8 shows the residuals between the AVHRR brightness temperature of the colder cluster and the IASI-convolved brightness temperature of the estimated cloud component for partially cloudy footprints (`ncl` = 2), using f_{IASI}. In contrast to the clear-sky case, the residuals exhibit a much larger spread, ranging from approximately −4 to +7 K, indicating significantly poorer agreement between the reconstructed and observed radiances.

The fitted gradients are negative (-0.169 ± 0.157 for Channel 4 and -0.193 ± 0.203 for Channel 5), but the large uncertainties indicate that any temperature dependence is weak. This suggests that the linear mixing model captures only the general behaviour of partially cloudy scenes, rather than reproducing the observed residuals accurately.

These discrepancies likely arise from the simplified assumptions of the model, including the representation of the footprint as a two-component system and the inability of the model to capture sub-footprint cloud variability, multi-layer cloud structure, and semi-transparent cloud effects. This behaviour is consistent with previous studies [3], which show that linear radiance mixing models can exhibit large errors in partially cloudy scenes due to the inhomogeneity of clouds.

4. *Using $f = f_{\mathrm{AVHRR}}$*

The analysis was repeated using the fraction of the colder AVHRR cluster, f_{AVHRR} in Eqn. 5.

Fig. 9 shows the residuals between AVHRR and IASI-convolved brightness temperatures for the cloud component in partially cloudy footprints using f_{AVHRR}. In contrast to results obtained using f_{IASI}, the agreement deteriorates significantly, with residuals between 0 and 35 K, indicating a large discrepancy between the reconstructed and observed radiances. This occurs because f_{AVHRR} is based on radiance clustering rather than physical cloud detection. As a result, the colder cluster may include semi-transparent or partially cloud-contaminated regions rather than representing a purely cloudy component.

The negative fitted gradients (-0.671 ± 0.093 for Channel 4 and -0.708 ± 0.082 for Channel 5) demonstrate a pronounced temperature-dependent bias. The residuals are large and positive at lower brightness temperatures and decrease towards zero at higher temperatures, indicating a systematic misrepresentation of the cloud contribution.

5. *Comparison of Cloud Fraction Methods*

To assess the performance of the two cloud fraction definitions, we compared the predicted IASI cloud component temperatures with the AVHRR mean brightness temperatures of the colder cluster. The mean bias and root-mean-square error (RMSE) for

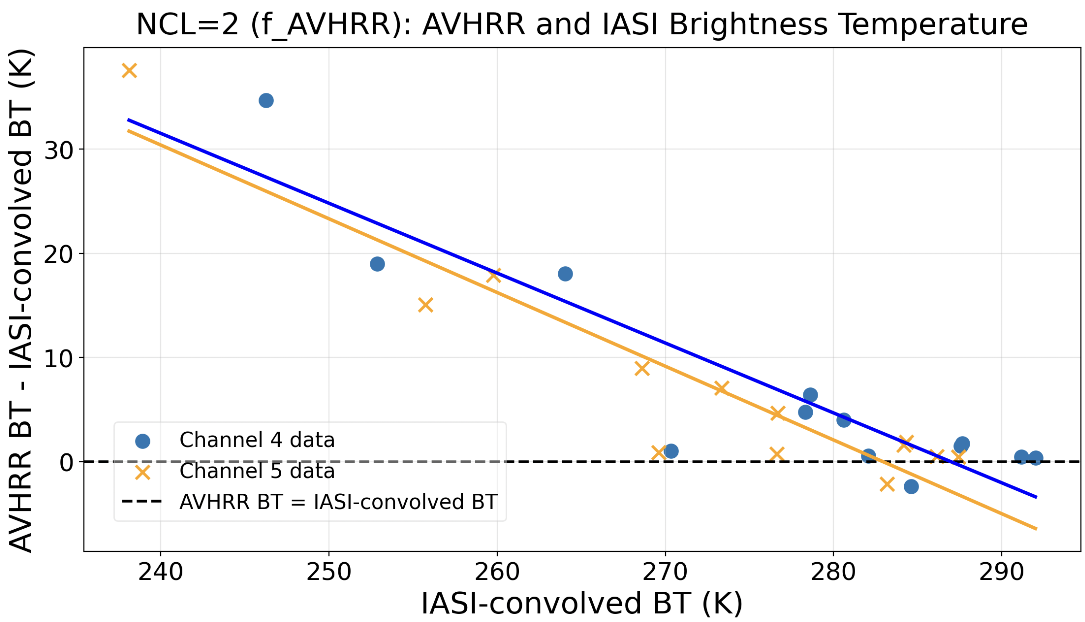

Figure 9: Brightness temperature (BT) residuals (AVHRR − IASI) for the cloud component in partially cloudy footprints (`ncl` = 2), plotted as a function of the IASI-convolved BT of the estimated cloud component using f_{AVHRR}. The AVHRR mean BT of the colder cluster is compared with the IASI BT obtained by inverting the linear radiance mixing model (Eqn. 5). Linear fits are shown for both channels: Channel 4: $\Delta T = (-0.671 \pm 0.093)\, T_{\mathrm{IASI}} + (192.6 \pm 25.8)$, Channel 5: $\Delta T = (-0.708 \pm 0.082)\, T_{\mathrm{IASI}} + (200.3 \pm 22.3)$.

the cases shown in Figs 8 (f_{IASI}) and 9 (f_{AVHRR}) are summarised in Table. 1.

Table 1: Mean bias and RMSE between predicted IASI cloud brightness temperatures and AVHRR colder-cluster brightness temperatures.

	Mean Bias (K)	RMSE (K)
Ch4, f_{IASI}	1.44	3.8
Ch5, f_{IASI}	1.54	4.0
Ch4, f_{AVHRR}	6.94	12.4
Ch5, f_{AVHRR}	7.32	12.8

The bias and RMSE values are substantially larger when using f_{AVHRR} compared to f_{IASI}, indicating that f_{IASI} provides a more reliable estimate of cloud fraction. The positive mean bias indicates that the AVHRR cloud brightness temperatures are systematically warmer than those predicted from IASI, consistent with the interpretation that the colder AVHRR cluster includes contributions from semi-transparent regions.

Channel 5 consistently exhibits slightly larger bias and RMSE than Channel 4. This is likely due to its greater sensitivity to atmospheric water vapour absorption within the infrared window region, which introduces additional variability and reduces the accuracy of the cloud radiance retrieval.

Overall, these results demonstrate that the IASI cloud fraction, f_{IASI}, provides a more accurate representation of the cloud component in the linear model than the AVHRR radiance cluster fraction, f_{AVHRR}.

VIII. DETERMINING THE OPTIMAL CLOUD FRACTION VALUE

A further extension of this study is to determine the value of cloud fraction f_{best} (Eqn. 6) that best reproduces the observed mixed IASI radiance under the assumption of linear radiance mixing.

We approximate the cloudy radiance component using the AVHRR mean radiance of the colder cluster. Rearranging Eqn. 3 gives the effective cloud fraction:

$$f_{\mathrm{best}} = \frac{L_{\tilde{\nu}}^{\mathrm{mix}} - L_{\tilde{\nu}}^{\mathrm{clear}}}{L_{\tilde{\nu}}^{\mathrm{cloud}} - L_{\tilde{\nu}}^{\mathrm{clear}}}, \quad (6)$$

where $L_{\tilde{\nu}}^{\mathrm{mix}}$ and $L_{\tilde{\nu}}^{\mathrm{clear}}$ are the convolved IASI radiances for the partially cloudy and clear-sky footprints, respectively, and $L_{\tilde{\nu}}^{\mathrm{cloud}}$ is the AVHRR mean radiance of the colder cluster.

The derived quantity f_{best} represents the cloud fraction required for the linear model to reproduce the observed mixed radiance. Since $L_{\tilde{\nu}}^{\mathrm{cloud}}$ is derived from AVHRR radiance clustering, f_{best} is inherently a radiance-weighted quantity rather than a purely geometric cloud fraction (like f_{IASI}).

Comparison with f_{AVHRR} shows reasonable linear agreement in both channels:

$$f_{\mathrm{best}} = (0.869 \pm 0.123)\, f_{\mathrm{AVHRR}} + 0.30 \quad \text{(Ch 4)},$$

$$f_{\text{best}} = (0.851 \pm 0.129)\, f_{\text{AVHRR}} + 0.31 \quad \text{(Ch 5)}.$$

This indicates that f_{AVHRR} is consistent with f_{best}, as both are based on the AVHRR radiance clustering algorithm.

Although f_{IASI} shows weaker agreement with f_{best} ($f_{\text{best}} = (0.588 \pm 0.351)\, f_{\text{IASI}} + 0.30$), results from Section VII show that it produces better agreement with observed brightness temperatures. This reflects the fact that f_{best} is derived using the AVHRR mean radiance of the colder cluster, whereas f_{IASI} is based on physical cloud detection. As a result, f_{IASI} is likely more representative of the true cloud distribution within the footprint, despite being less consistent with the model assumptions.

Overall, the IASI-derived cloud fraction (f_{IASI}) provides better agreement with observations, while the AVHRR-derived fraction (f_{AVHRR}) is more consistent with the assumptions of the linear mixing model. This highlights both the ambiguity in defining cloud fraction and the strong dependence of the model on its choice.

IX. CONCLUSION

This study assessed whether AVHRR-derived cloud information can be used to model partial cloud contamination in IASI radiances using a linear radiance mixing framework. Clear-sky comparisons show close agreement between convolved IASI and AVHRR brightness temperatures, validating the consistency between the two instruments.

In partially cloudy scenes, the assumption that a neighbouring clear-sky footprint represents the clear component is broadly valid, but introduces a systematic bias. The radiance mixing model was tested using two cloud fractions: a physically based IASI fraction (f_{IASI}) and a radiance-clustering fraction (f_{AVHRR}). The IASI cloud fraction produces cloud-component radiances that agree more closely with the AVHRR mean radiance of the colder cluster, whereas the clustering-based fraction f_{AVHRR} performs significantly worse in reproducing observed brightness temperatures. This demonstrates that radiance-based classification does not reliably represent physical cloud cover.

Clouds exhibit significant spatial variability in optical depth, temperature, and vertical structure, meaning that a single cloud fraction cannot fully represent their radiative impact. Future work could focus on incorporating additional cloud properties, such as optical thickness, to better represent this variability.

The linear model captures the general behaviour of partially cloudy scenes, but its accuracy is strongly limited by how cloud fraction is defined. The IASI-derived cloud fraction (f_{IASI}) provides a more representative estimate of the cloud radiance, whereas the AVHRR-derived fraction (f_{AVHRR}) is more consistent with the assumptions of the linear mixing model. This highlights the inherent difficulty in representing cloud fraction within simplified radiative frameworks, and suggests that improving cloud fraction estimates is key to increasing the use of partially cloudy observations in retrieval algorithms.

Acknowledgements. The author thanks Dr Anu Dudhia for supervising this project and the members of the Earth Observation Data Group for their support.

REFERENCES

[1] J. Yang, P. Gong, R. Fu, M. Zhang, J. Chen, S. Liang, B. Xu, J. Shi, and R. Dickinson. The role of satellite remote sensing in climate change studies. *Nature Climate Change*, 3:875–883, 2013. doi: 10.1038/nclimate1908.

[2] D. G. Feist, S. G. Arnold, F. Hase, et al. On the use of iasi spectra to retrieve cloud properties. *Atmospheric Chemistry and Physics*, 14:5599–5613, 2014. doi: 10.5194/acp-14-5599-2014.

[3] Adrian Doicu, Dmitry S. Efremenko, Diego Loyola, and Thomas Trautmann. Approximate models for broken clouds in stochastic radiative transfer theory. *Journal of Quantitative Spectroscopy and Radiative Transfer*, 145:74–87, 2014. ISSN 0022-4073. doi: 10.1016/j.jqsrt.2014.04.025.

[4] Dmitry Efremenko, Adrian Doicu, Diego Loyola, and Thomas Trautmann. Fast stochastic radiative transfer models for trace gas and cloud property retrievals under cloudy conditions. In Alexander Kokhanovsky and Gerrit de Leeuw, editors, *Springer Series in Light Scattering: Volume 1: Multiple Light Scattering, Radiative Transfer and Remote Sensing*, volume 1 of *Springer Series in Light Scattering*, pages 231–277. Springer International Publishing, 2018. ISBN 978-3-319-70796-9. doi: 10.1007/978-3-319-70796-9_3.

[5] EUMETSAT. Basic satellite channels and absorption bands, n.d. URL `https://resources.eumetrain.org/data/Basic_Channels/print.htm`. Accessed: 2026-04-03.

[6] Rttov coefficient information: Metop-3 avhrr srf, n.d. URL `https://nwp-saf.eumetsat.int/downloads/rtcoef_info/visir_srf/rtcoef_metop_3_avhrr_srf.html`. Accessed: 2026-04-08.

A. GEOGRAPHIC CLOUDY REGIONS

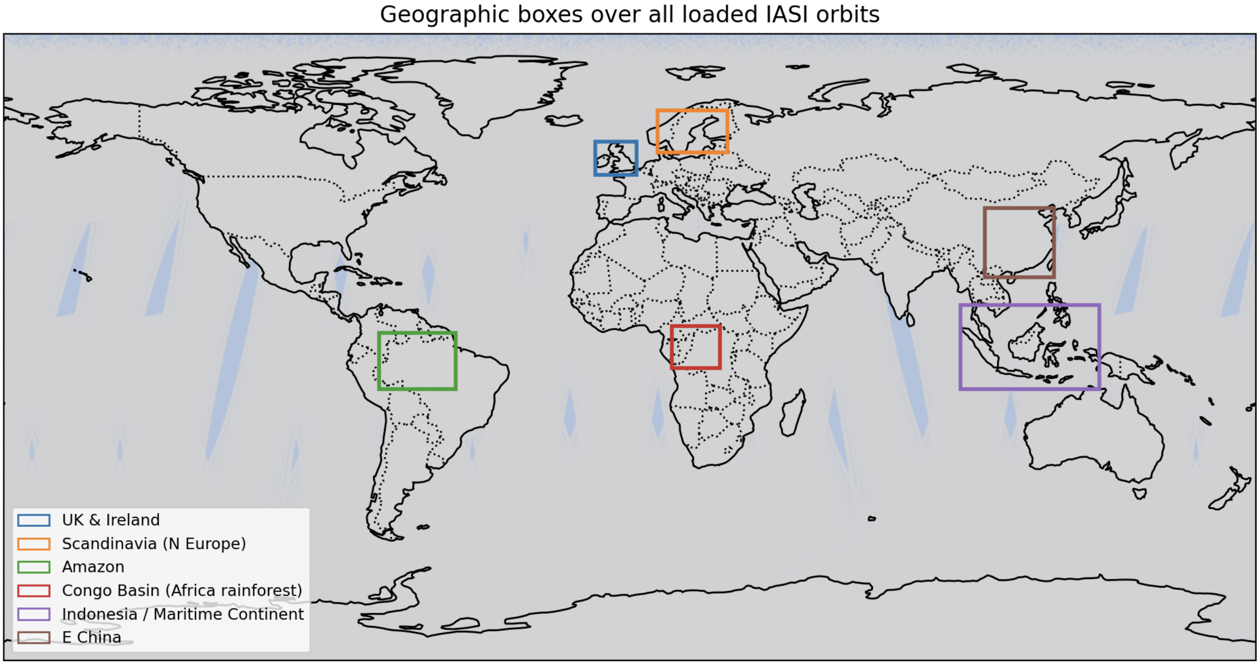

Figure 10: Geographic regions of interest used for the motivation in this study, selected for their typically high cloud coverage (e.g. Scandinavia, Amazon, Maritime Continent).

Table 2: Latitude and longitude boundaries used for the boxes in Fig. 10.

Region	Lat_{min}	Lat_{max}	Lon_{min}	Lon_{max}
UK & Ireland	49.5	59.0	-10.0	2.0
Scandinavia (N Europe)	56.0	68.0	8.0	28.0
Amazon	-12.0	4.0	-72.0	-50.0
Congo Basin	-6.0	6.0	12.0	26.0
Indonesia / Maritime Continent	-12.0	12.0	95.0	135.0
East China	20.0	40.0	102.0	122.0

List of all files used to generate Fig. 10:

```
IASI_xxx_1C_M03_20220113225656Z_20220114004152Z_N_O_20220114003755Z.nat
IASI_xxx_1C_M03_20220114004152Z_20220114022359Z_N_O_20220114022150Z.nat
IASI_xxx_1C_M03_20220114022400Z_20220114040559Z_N_O_20220114040446Z.nat
IASI_xxx_1C_M03_20220114054800Z_20220114072959Z_N_O_20220114072837Z.nat
IASI_xxx_1C_M03_20220114073000Z_20220114091159Z_N_O_20220114090953Z.nat
IASI_xxx_1C_M03_20220114091200Z_20220114105359Z_N_O_20220114105103Z.nat
IASI_xxx_1C_M03_20220114105400Z_20220114123255Z_N_O_20220114123146Z.nat
IASI_xxx_1C_M03_20220114123256Z_20220114141455Z_N_O_20220114141128Z.nat
IASI_xxx_1C_M03_20220114141456Z_20220114155359Z_N_O_20220114155152Z.nat
IASI_xxx_1C_M03_20220114155400Z_20220114173255Z_N_O_20220114173142Z.nat
IASI_xxx_1C_M03_20220114173256Z_20220114191455Z_N_O_20220114191211Z.nat
IASI_xxx_1C_M03_20220114191456Z_20220114205359Z_N_O_20220114205328Z.nat
IASI_xxx_1C_M03_20220114205400Z_20220114223559Z_N_O_20220114223426Z.nat
IASI_xxx_1C_M03_20220114223600Z_20220115001759Z_N_O_20220115001645Z.nat
```

B. IASI AND AVHRR FLAGS

Table 3 summarises the main flags provided in the IASI data for each field of view. Each IASI footprint can be uniquely labelled by `lin`, `istp` and `ifov`.

Flag	Description
`lin`	Scan line index
`istp`	Across track position index
`ifov`	Instantaneous field of view
`cld`	AVHRR cloud fraction (%)
`lnd`	AVHRR land fraction (%)
`ncl`	Number of radiance clusters in the footprint
`rav`	Average radiance of a chosen cluster
`pct`	Percentage of that cluster in the footprint

Table 3: Description of IASI and AVHRR data flags.